Asian Journal of Chemistry; Vol. 36, No. 1 (2024), 135-140

ASIAN JOURNAL OF CHEMISTRY

https://doi.org/10.14233/ajchem.2024.30718

Multifunctional Properties of Biphasic $DyFeO_3$ Perovskite/$Dy_3Fe_5O_{12}$ Garnet Rare Earth Orthoferrite

T. PUNITHA[1,*], P. BALAMURUGAN[1] and G. SATHISH KUMAR[2]

[1]PG & Research Department of Physics, Government Arts College (Men), Nandanam, Chennai-600035, India
[2]Department of Physics, Sri Sai Ram Engineering College, Chennai-600044, India

*Corresponding author: E-mail: punithathiruvengadam11@gmail.com

Received: 16 October 2023; *Accepted*: 19 November 2023; *Published online*: 31 December 2023; AJC-21495

Rare-earth orthoferrites are a group of compounds which exhibit improved magnetic, optical, and electrical characteristics throughout a wide range of temperatures. In present work, dysprosium based orthoferrite compound containing double phase of $DyFeO_3$ perovskite/$Dy_3Fe_5O_{12}$ garnet was synthesized *via* co-precipitation technique. A mixed phase of orthoferrite, $DyFeO_3$ perovskite and $Dy_3Fe_5O_{12}$ garnet has been obtained. The X-ray diffraction (XRD) was carried out to explore the structural arrangements of atoms in the prepared material and clearly demonstrated the presence of both cubic phase of $Dy_3Fe_5O_{12}$ (bcc) and orthorhombic phase of $DyFeO_3$ in the powder sample. The nanoparticles surface morphological behaviour is explored with field emission scanning electron microscope (FE-SEM), which shows nearly spherical shape particles with little agglomeration. Using the UV-visible absorbance, band gap of the prepared sample was evaluated as 2.06 eV from Tauc plot. The magnetization behaviour was observed using a vibrating sample magnetometer (VSM), which revealed the Langevin component (ferromagnetic) at low field and as linear component (antiferromagnetic) at high field. The electric polarization (P-E loop) studies also revealed the typical induced ferroelectric behaviour.

Keywords: Co-precipitation, Rare-earth orthoferrites, Nanocomposite, Magnetic property, Electric polarization.

INTRODUCTION

The discovery of new materials with diverse functionalities is greatly encouraged by the emergence of the various characteristics in single/multiphase compounds. Multiferroics are the materials that include both magnetism and ferroelectricity in the same composition. They present a viable method for developing multipurpose devices where the charges can be managed by a magnetic field and the spins may be affected by a voltage. Rare-earth orthoferrite ($ReFeO_3$) takes perovskite configuration with orthorhombic space group *Pbnm*. It exhibits ferroelectricity, ferromagnetism, piezoelectricity and magnetoelectric coupling and can be classified as multiferroic materials [1]. Many multiferroic materials such as $ReFeO_3$ (Re = La, Pr, Nd, Sm, Gd) [2], $BiMnO_3$, $BiFeO_3$ and $TbMnO_3$ are investigated in the past decades due to their simultaneous occurrence and coupling effects of ferroelectric and magnetic properties for technological developments [3,4]. The inorganic, single phase, multiferroic material bismuth ferrite ($BiFeO_3$, BFO) is one of them and exhibits both ferroelectric and magnetic characteristics at ambient temperature. One of the most thoroughly studied multiferroic compounds is BFO, in which partially filled *d*-orbital of iron causes magnetic ordering and the 6*s*-electrons of Bi are responsible for ferroelectricity. The structure of $BiFeO_3$ is rhombohedral when it is at normal temperature conditions. The perovskite (ABO_3) structure of BFO belongs to the *R*3*c* phase group [5].

Bismuth ferrite shows a maximum remnant polarization value and useful for ferroelectric capacitor devices [1]. Due to Bi volatilization, oxygen vacancies, impurity phases and valence fluctuation of Fe ions, there are a number of issues to be concerned about, including coercive field, leakage current density, resistivity and low fatigue resistance. Doping methods were applied to solve these problems. To increase chemical stability, reduce oxygen vacancy concentration and lower leakage current, rare-earth ions were substituted on the A or B site [6]. It is a fact that perovskites are crucial to the development of photonics, optoelectronics and the energy industries. Additionally, the perovskites were able to develop optoelectronic and photovoltaic applications because to their special physical characteristics,

such as long-range charge transport mechanisms, high absorption coefficients, ferroelectricity, low exciton binding energies, high dielectric constant, *etc.* [7,8].

Although substantial magnetoelectric coupling has been demonstrated in composite materials, single-phase materials are still not fully understood. The magnetoelectric coupling is typically either absent or extremely weak in single-phase materials. Currently, a significant and rapidly evolving area of research focuses on developing magnetoelectric materials that have a strong coupling effect at normal room temperature. For storing hydrogen energy, binary metal oxides (BMOs) with unique structural features have also been reported [9-12]. The presence of structural flaws and the development of stable chemical interactions between protons and oxygen, BMOs can adsorb hydrogen [13].

Several $ReFeO_3$ have been reported in the literature as multiferroics materials. The $DyFeO_3$ has magnetic ordering driven multiferroic characteristics below 4 K [14,15]. It is observed that $DyFeO_3$ and $BiFeO_3$ have the same crystal structure [9-11] and $DyFeO_3$ is of particular interest since the spin reorientation is classified as a Morin transition with the transition temperature depending strongly on Dy-Fe interaction. Garnet ($Dy_3Fe_5O_{12}$) and dysprosium iron perovskite ($DyFeO_3$) are the two separate entities, studied for variety of industrial applications [16]. Various methods such as solid-state [17], sol-gel [18] and pulsed laser deposition [19], are used for the synthesis of $DyFeO_3$, whereas hydrothermal [20] and ball-mill methods are used for the preparation of $Dy_3Fe_5O_{12}$ nanoparticles [21]. Besides, there are only few reports on the synthesis and properties of dysprosium based orthoferrite and the effect of *f*-block elements on its crystal properties. In this work, simple and cost effective co-precipitation technique is employed to synthesize the multiferroic material and these materials find applications in hydrogen storage [22]. In present study, dysprosium based orthoferrite ($DyFeO_3$), novel multiferroic material has been synthesized to evaluate their microstructural, magnetic, optical and P-E studies.

EXPERIMENTAL

Ferric nitrate nonahydrate ($Fe(NO_3)_3{\cdot}9H_2O$), dysprosium nitrate $Dy(NO_3)_3{\cdot}5H_2O$, polyethylene oxide, ammonia were used for the preparation of $DyFeO_3$ material using co-precipitation route. In brief, iron nitrate and dysprosium nitrate were separately dissolved in deionized water and then mixed together. The mixed solution was heated slowly to reach 80 ºC and the polyethylene oxide was added to the solution and stirred the solution vigorously for 2 h follwed by the addition of ammonia solution dropwise. Subsequently, the sample was cooled to room temperature and washed 5 times with deionized water followed by ethanol using centrifugation. The sample was dried at 200 ºC and then annealed at 1200 ºC for 5 h to investigate the microstructural, optical and magnetic properties. The powder sample was made into cylindrical pellets using hydraulic press and sintered at a temperature of 500 ºC and used for P-E studies.

Characterization: Bruker AXS diffractometer D8 Advance, XRD patterns were captured using CuK1 radiation in the 2θ range of 10-80º. FT-IR Shimadzu spectrophotometer, used to obtain FT-IR spectra in the 4000-400 cm^{-1} range. A Philips XL-30 FESEM was used to gather the FESEM images in order to examine the surface morphology of the particles. The optical studies were conducted with Shimadzu UV-Visible-NIR spectrophotometer UV-3600 plus, additionally, a vibrating sampling magnetometer (VSM, Model 7400-Lake Shore) was used to study the magnetic properties. The electrical polarization (P-E) behaviour was traced with PE loop tracer.

RESULTS AND DISCUSSION

X-ray diffraction (XRD) studies: The sample was analyzed using X-ray diffractometer in the 10-80º range with the step size of 0.02º/s and the observed pattern is shown in Fig. 1. The XRD pattern shows the intensity peaks at (2θ) angles 17.57º, 26.94º, 28.85º, 32.27º, 35.50º, 39.86º, 45.08º, 51.06º, 53.34º, 55.47º, 59.73º, 69.46º, 84.03º corresponds to (211), (321), (400), (420), (422), (521), (611), (444), (640), (642), (800), (842) and (140) intensity planes, respectively and demonstrates the presence of $Dy_3Fe_5O_{12}$ garnet phase and found to be matched with the card no. JCPDS # 23-0237. From the diffraction pattern, it was observed that $DyFeO_3$ phase exhibits distinct intensity maxima at specific angles, namely 23.3º (002), 25.98º (111), 33.3º (112), 47.4º (220), 49.0º (221) and 64.4º (133). These findings provide confirmation of the orthorhombic phase of $DyFeO_3$ (JCPDS #47-0069) as previously reported by Salehabadi *et al.* [22] and Sivakumar *et al.* [23].

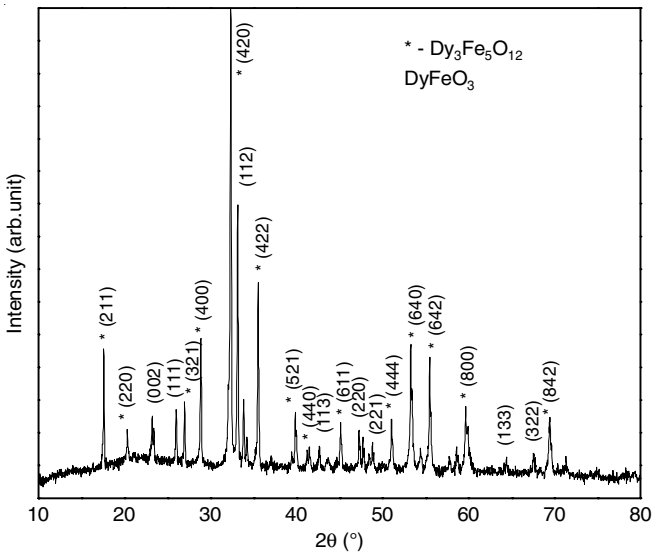

Fig. 1. XRD pattern of dysprosium orthoferrite

For $Dy_3Fe_5O_{12}$, an orthorhombic *Pbnm* space group, but for $DyFeO_3$ perovskite oxides, a cubic crystal structure which belongs to *Ia3d* space group. It is reported that at higher temperature, the incorporation of precursors (dysprosium nitrate and ferrite nitrate) mostly favours to the formation of $DyFeO_3$ orthoferrite structure. At the same time, due to excess incorporation of ferric ions in to the parent $DyFeO_3$ system leads to the mixed phase formation of $Dy_3Fe_5O_{12}$ (garnet phase) with $DyFeO_3$ (orthoferrite phase) [24]. The identified mixed phase formation may be due to the mere incorporation of lower ionic radii Fe^{3+} (0.68 Å) ion into the $DyFeO_3$ system, Hence, the condition

reveals that the content of Fe is critical to achieve single phase formation of $DyFeO_3$ structure and the same was established with no more evidences of Fe rich secondary phases in the X-ray diffraction planes.

The mean crystallite size was computed from the FWHM of the (4 2 0) ($DyFeO_3$) peak of the XRD pattern using Scherrer's equation:

$$D = \frac{0.9\lambda}{\beta\cos\theta} \quad (1)$$

where k = 0.9, λ stands for monochromatic X-ray wavelength, β is the full width at half maximum (FWHM) of the peak, θ is the wavelength of radiation. The estimated crystallite size is found to be around 27 nm.

As the proportion of Dy^{3+} was increased to 25.0%, several new peaks appeared at 33.16º, 40.70º, 49.33º, 53.99º, 57.52º, 62.39º and 64.17º (JCPDS: 25-1402). Similarly, the excessive addition of dysprosium or introduction into the reactive system has replaced some iron in Fe_2O_3 crystal to form $DyFe_{4.5}O_6$ orthoferrite nanoparticles, which have the similar structure to the $RFeO_3$ type $Dy_{0.75}Fe_{1.25}O_3$ orthoferrite nanoparticles. According to the XRD measurements, Dy_3Fe5O_{12} and $DyFeO_3$ phases were formed.

FTIR studies: The FTIR spectrum (Fig. 2) shows the bands at 2350, 2140, 1960, 1580, 1080, 811, 588 and 559 cm^{-1}. The stretching vibration modes of the Fe-O can be used to explain the absorption bands at 559 and 588 cm^{-1}. The oxygen-metal-oxygen (O-M-O) bending modes and metal-oxygen (M-O) stretching vibrations are present in several strong bands in the structures between 500 and 800 cm^{-1}. The bands between 500 and 800 cm^{-1} indicate the stretching vibrations of metal-oxygen (Dy-O, Fe-O) and metal-oxygen-metal (M-O-M). It is significant to remember that at around 559 cm^{-1}, Dy-O also forms its symmetrical stretching vibration. It is possible to attribute the stretching vibration and bending vibration of OH groups at 1580 cm^{-1} [22].

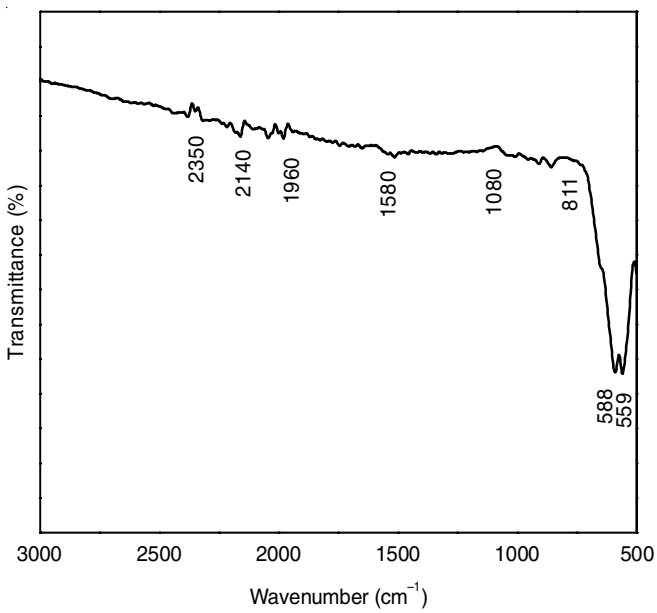

Fig. 2. FTIR spectrum of the dysprosium orthoferrite

Surface morphology: The surface topography of compound is investigated using the FE-SEM with different magnifications. It shows the well-defined formation of crystallites in the nanoscale and the nanoparticles are formed inhomogeneously (Fig. 3). The crystallites are very dense and are of different sizes. The topography shows nearly spherical shape particles with some agglomeration. The set of crystallites appears white and other crystallites appear black. This is due to the difference of different atomic numbers of Fe and Dy. The EDX analysis confirmed the presence of Fe, Dy and O elements in the sample (Fig. 4). The percentage (atomic) of Dy, Fe and O in the sample were 18.55, 23.94, 57.50, respectively. It can be observed from Dy, Fe and O elements are uniformly distributed in the sample [22].

Optical studies: UV-visible spectrophotometer was used to characterize the optical properties of the sample in the 300-1000 nm wavelength range. The optical absorption of the sample is shown in Fig. 5a, where the curve invariably shows that the absorbance is increased sharply in the visible region (~ 580 nm) and decreases with increasing wavelength.

The absorption coefficient, α (ω) was determined using the relation:

$$\alpha = 2.303(A) \quad (2)$$

where 'A' is the absorbance of the nanoparticles.

The absorption coefficient varies with the incident photon energy (hν) and has the following formula near the absorption edge, according to the theory of optical transitions (direct or indirect) in solids.

$$\alpha h\nu = A(h\nu - E_g)^n \quad (3)$$

where "n" is dependent on the type of optical transitions and A is a constant; E_g is the band gap.

The prepared nanomaterial optical bandgaps were also computed. The linear portion of the intercept on energy (x) axis from the Tauc plot (Fig. 5b), is extrapolated to yield the direct bandgap. According to the optical investigations, the bandgap of 2.06 eV is obtained for this material, which is almost similar to the reported value [25].

Magnetic properties: At ambient temperature, the field range of 15 kGH was used to measure the field dependent magnetization (M-H) of Dy-Fe-O (Fig. 6). The sample's saturation magnetization, remanent magnetization and coercivity values were 86.11 ($M_s \times 10^{-3}$) emu/g, 24.53 ($M_r \times 10^{-3}$) emu/g and 509 Oe, respectively. When the magnetic field is reduced, the magnetization rises significantly, indicating the coexistence of magnetic phases. The magnetization then rises gradually as the magnetic field increases. The measured M-H curve suggested that the magnetization at low fields tends to saturate, whereas the magnetization at high fields manifestly displays unsaturated open linearity. The uncompensated moment of the particle core is related to the saturating part, while the spins of the disordered surface are associated to the non-saturating part. This is comparable to the core-shell magnetic structure of NiO nanoparticles, with the core as antiferromagnetic ordering and the shell as ferromagnetic response [26]. This work reveals that the antiferromagnetic component produces a linear dependence whereas the ferromagnetic component follows the Langevin pattern. The

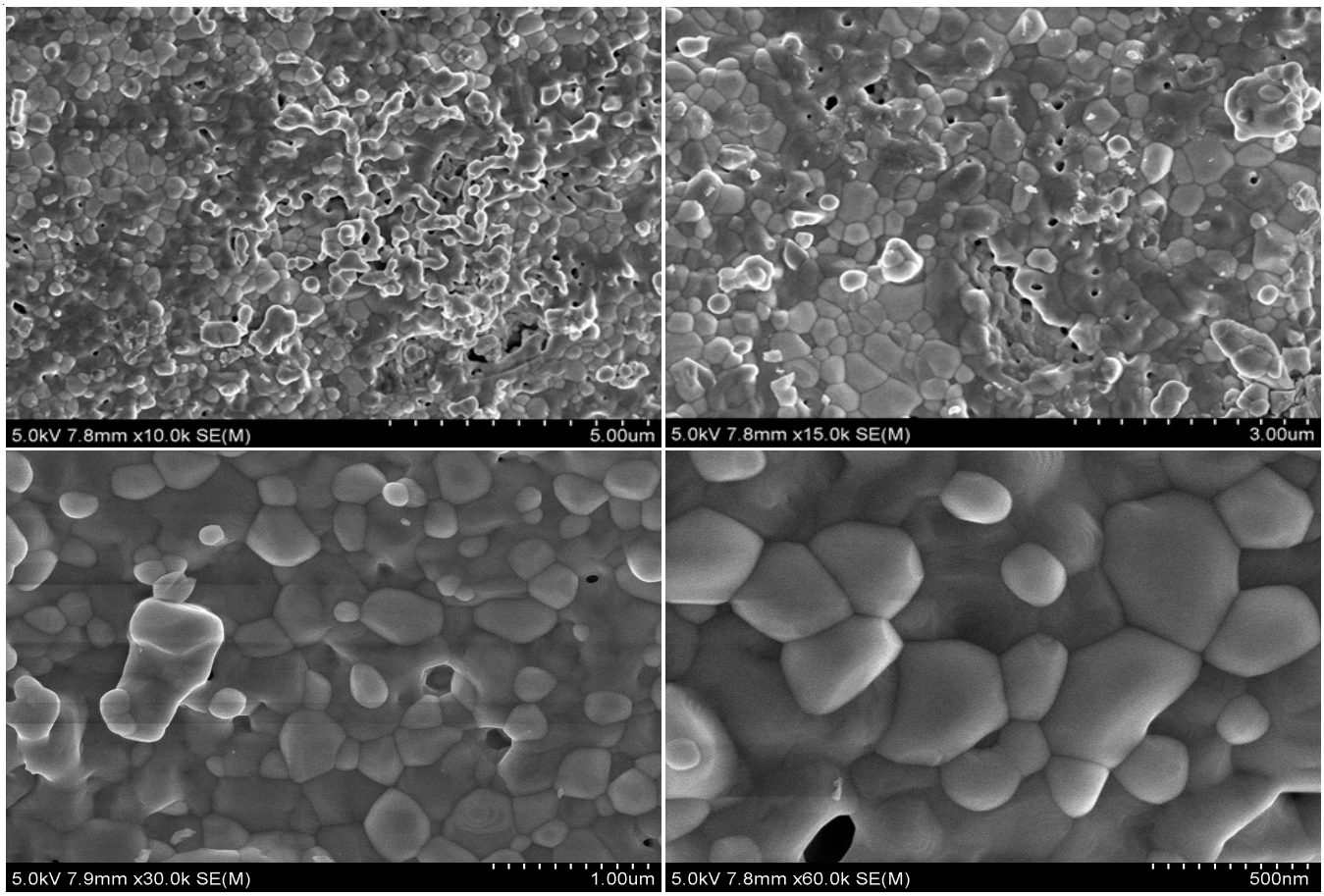

Fig. 3. Surface morphology of the orthoferrite at different magnification

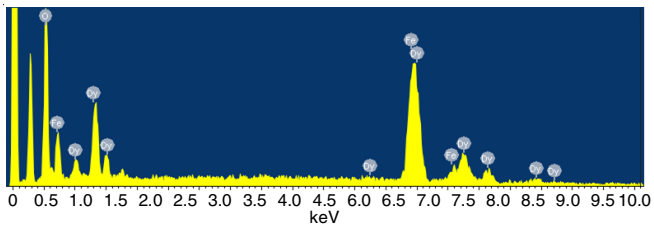

Fig. 4. EDAX of the prepared orthoferrite

initial magnetic field in this study can be characterized by the ferromagnetic Langevin component, but in the high-field region, it is characterized by the linear component, which is antiferromagnetic in nature. Hence, the magnetization (M) for an applied field (H) at room temperature T is given by:

$$M = M_0 + \chi_{AF} H \quad (4)$$

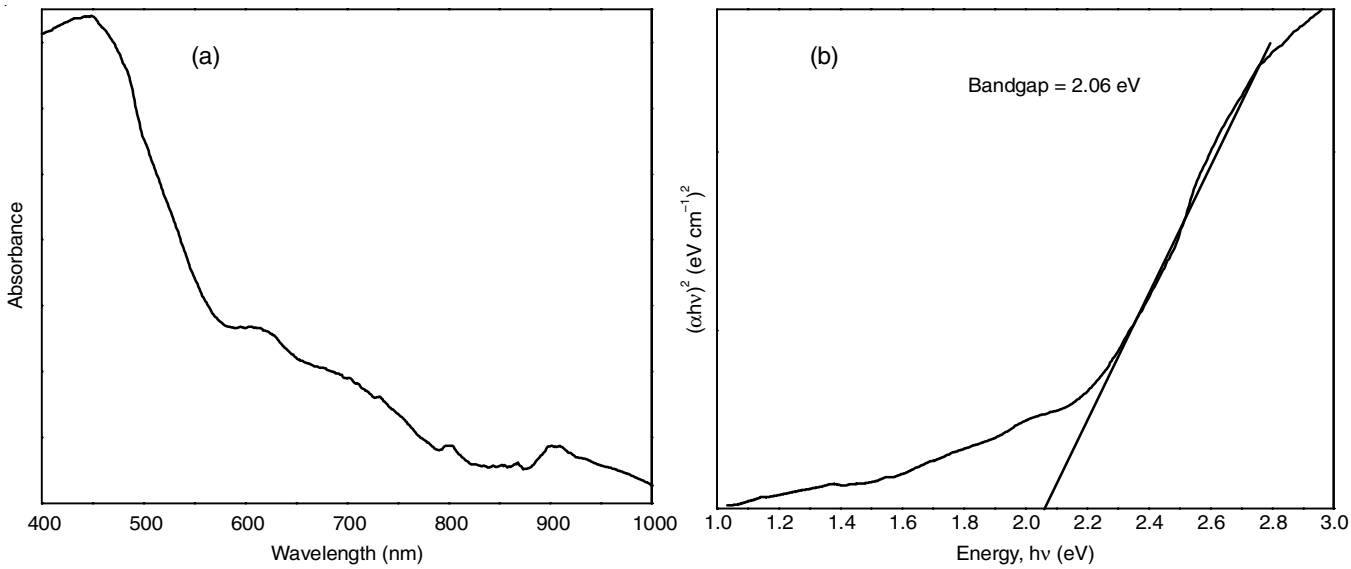

Fig. 5. (a) Absorbance spectrum of the orthoferrite sample; (b) Tauc plot for finding the band gap of the prepared composite

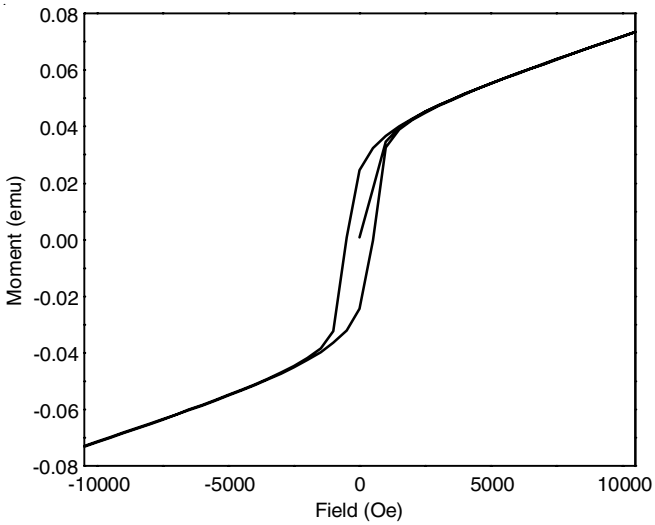

Fig. 6. Magnetization (M-H) curve for orthoferrite sample

The non-compensation of the surface spins is responsible for M_0's rapid increase in magnetization and AF H's antiferromagnetic contribution is responsible for AF H's non-saturate magnetization at high fields. replacing M_0, which is dependent on the surface component,

$$M = Ms\left[\coth\left(\frac{\mu H}{k_B T}\right) - \frac{k_B T}{\mu H}\right] + \chi_{AF} H \qquad (5)$$

where, k_B = Boltzmann's constant, μ = non-compensated magnetic moment, AF = antiferromagnetic susceptibility and Ms = saturation magnetization. The greater coercivity value shows that the non-compensated surface spins are primarily responsible for the magnetization of the sample.

There is debate regarding the causes of the ferromagnetism that occurs in metal oxide nanostructures and it has been found that a variety of defects and vacancies are to blame. According to a report, oxygen vacancies, tin vacancies and tin interstitials caused room-temperature ferromagnetism to be seen in SnO_2 nanostructures [27]. Furthermore, the room-temperature ferromagnetism is also present in ZnO nanoparticles because of surface flaws such oxygen vacancies, zinc vacancies and zinc interstitials [28]. As previously reported, capping these flaws with suitable organic molecules results in changes to the electrical structure and controllable ferromagnetic behaviour in the ZnO and SnO_2 nanostructures [27].

Electric polarization (P-E) analysis: In order to analyze the ferroelectric behaviour of the orthoferrites at room temperature, electric polarization was carried out and the observed polarization pattern is shown in Fig. 7. It is inferred that the sample displayed an unsaturated ferroelectric behaviour. Furthermore, it is observed that with the increase of field strength leads with increase of loop area, which defines the improving polarizability of the compound. It was also observed that the replacement of Dy^{3+} ions at the Fe^{3+} site in Fe_2O_3 leads with inducement of ferroelectric behaviour and the area of hysteresis loop suggests that the compound has near saturation behaviour, which is a very peculiar and quite acceptable characteristic feature for a ferroelectric material with induced ferroic behaviour [29].

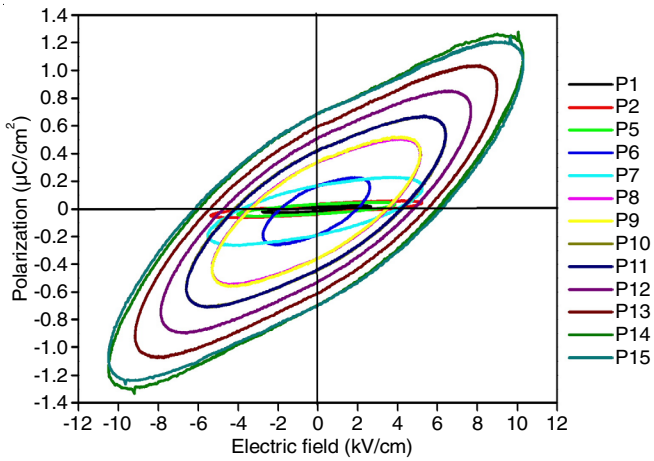

Fig. 7. Ferroelectric hysteresis loop of orthoferrite

It is known that changes in composition, microstructure and defects within the crystal structure of the materials have a major impact on ferroelectric characteristics. Hence, it was also observed that the mixing of Dy^{3+} ion into Fe_2O_3 host lattice leads to structural deformation and inducement of spontaneous dipole moment, which is responsible for ferroelectric behaviour. The identification of ferroelectric property in ε-Fe_2O_3 epitaxial thin film has been reported whereas there is no clear evidence of inducing ferroelectric property in Fe_2O_3 compound has been reported [30]. Hence, the present work reveals the possibility of inducing multiferroicity in the Fe_2O_3 compound.

The ferroelectric hysteresis loop exhibits non-zero remanance and coercivity values as the applied electric field is increased from 2 kV/cm to 10 kV/cm. Additionally, linear increases in the polarization values result in maximum polarization (P_{max}) of 1.2 C/cm^2, remanant polarization (Pr) of 0.7 C/cm^2 and coercivity (Ec) of about 6 kV/cm, which reveals the ideal ferroelectric behaviour. Due to the reduced resistivity under the room temperature conditions, the lower resistance result reveals the sample's leaky nature. Although the saturation polarization P_{max} (1.2 C/cm^2) was found to be less and the change of the hysteresis loop shows that the sample is loose. The reported value is extremely compatible with that of comparable simple perovskite-related compounds [23]. The possibility of developing ferroelectric behaviour when adding Dy^{3+} ions into the ferromagnetic Fe_2O_3 compound has been found *via* the P-E loop analysis.

Conclusion

In this work, the co-precipitation method was employed for preparing pure dysprosium orthoferrite nanostructures. The microstructure, optical, magnetic and electric polarization studies were carried out. The structural and morphological observations provide enough proof for the mixed phase formation of $Dy_3Fe_5O_{12}$ and $DyFeO_3$ nanoparticles. XRD studies indicated the formation of $Dy_3Fe_5O_{12}$ and $DyFeO_3$ nanoparticles with cubic and orthorhombic structure, respectively. The crystallite size was found to be 27 nm for cubic structure. The FE-SEM images show the formation of crystallites with different sizes. The magnetic properties of $DyFeO_3$ were analyzed using a vibrating sample magnetometer (VSM) at 300 K. The P-E loop

analysis was used to determine the possibility of generating ferroelectric behaviour. The findings can be used to better understand rare-earth orthoferrite applications and the nature of magnetic interactions in these structures.

ACKNOWLEDGEMENTS

The authors thank Dr. Vasudevan, Chairman, Prince Shri Venkateshwara Arts and Science College, Chennai, India for providing the research facilities and continuous support for the research work. Thanks are also due to The Head, Department of Physics, B.S. Abdur Rahman Crescent Institute of Science and Technology, Chennai, India for sample analysis.

CONFLICT OF INTEREST

The authors declare that there is no conflict of interests regarding the publication of this article.

REFERENCES

1. D. Carranza-Celis, A. Cardona-Rodríguez, J. Narváez, O. Moscoso-Londono, D. Muraca, M. Knobel, N. Ornelas-Soto, A. Reiber and J.G. Ramírez, *Sci. Rep.*, **9**, 3182 (2019); https://doi.org/10.1038/s41598-019-39517-3
2. M. Nakhaei and D. Sanavi Khoshnoud, *Physica B*, **612**, 412899 (2021); https://doi.org/10.1016/j.physb.2021.412899
3. P.K. Gupta, S. Ghosh, A. Pal, S. Roy, A.G. Joshi, A.K. Ghosh and S. Chatterjee, *SN Appl. Sci.*, **1**, 1607 (2019); https://doi.org/10.1007/s42452-019-1640-8
4. S. Hanif, M. Hassan, S. Riaz, S. Atiq, S.S. Hussain, S. Naseem and G. Murtaza, *Results Phys.*, **7**, 3190 (2017); https://doi.org/10.1016/j.rinp.2017.08.061
5. C. Prakash, A.K. Yadav and A. Dixit, *Phys. Chem. Chem. Phys.*, **25**, 19868 (2023); https://doi.org/10.1039/D3CP02235H
6. C.M. Raghavan, J.W. Kim and S.S. Kim, *Ceram. Int.*, **39**, 3563 (2013); https://doi.org/10.1016/j.ceramint.2012.10.182
7. N.S. Kumar, R.P. Suvarna, K.C. Babu Naidu, P.P. Mohapatra and P. Dobbidi, *Inorg. Chem. Commun.*, **149**, 110408 (2023); https://doi.org/10.1016/j.inoche.2023.110408
8. N. Suresh Kumar and K. Chandra Babu Naidu, *J. Materiomics*, **7**, 940 (2021); https://doi.org/10.1016/j.jmat.2021.04.002
9. S. Sahoo, P.K. Mahapatra, R.N.P. Choudhary, M.L. Nandagoswami and A. Kumar, *Mater. Res. Express*, **3**, 065017 (2016); https://doi.org/10.1088/2053-1591/3/6/065017
10. Y. Tokunaga, S. Iguchi, T. Arima and Y. Tokura, *Phys. Rev. Lett.*, **101**, 097205 (2008); https://doi.org/10.1103/PhysRevLett.101.097205
11. G. Deng, Y. Chen, M. Tao, C. Wu, X. Shen, H. Yang and M. Liu, *Electrochim. Acta*, **55**, 1120 (2010); https://doi.org/10.1016/j.electacta.2009.09.078
12. A.T.S. Sudandararaj, G. Sathish Kumar, M. Dhivya, R.D. Eithiraj and I.B. Shameem Banu, *J. Alloys Compd.*, **783**, 393 (2019); https://doi.org/10.1016/j.jallcom.2018.11.205
13. S. Mathur, H. Shen, A. Leleckaite, A. Beganskiene and A. Kareiva, *Mater. Res. Bull.*, **40**, 439 (2005); https://doi.org/10.1016/j.materresbull.2004.12.002
14. Z.Y. Zhao, X. Zhao, H.D. Zhou, F.B. Zhang, Q.J. Li, C. Fan, X.F. Sun and X.G. Li, *Phys. Rev. B Condens. Matter Mater. Phys.*, **89**, 224405 (2014); https://doi.org/10.1103/PhysRevB.89.224405
15. F.K. Chiang, M.W. Chu, F.C. Chou, H.T. Jeng, H.S. Sheu, F.R. Chen and C.H. Chen, *Phys. Rev. B Condens. Matter Mater. Phys.*, **83**, 245105 (2011); https://doi.org/10.1103/PhysRevB.83.245105
16. A. Stroppa, M. Marsman, G. Kresse and S. Picozzi, *New J. Phys.*, **12**, 093026 (2010); https://doi.org/10.1088/1367-2630/12/9/093026
17. B.M. Wanklyn, D. Midgley and B.K. Tanner, *J. Cryst. Growth*, **29**, 281 (1975); https://doi.org/10.1016/0022-0248(75)90172-4
18. S.S.K. Reddy, N. Raju, C.G. Reddy, P.Y. Reddy, K.R. Reddy and V.R. Reddy, *J. Magn. Magn. Mater.*, **396**, 214 (2015); https://doi.org/10.1016/j.jmmm.2015.08.038
19. S.J. Luo, S.Z. Li, N. Zhang, T. Wei, X.W. Dong, K.F. Wang and J.-M. Liu, *Thin Solid Films*, **519**, 240 (2010); https://doi.org/10.1016/j.tsf.2010.08.002
20. G. Rekha, R. Tholkappiyan, K. Vishista and F. Hamed, *Appl. Surf. Sci.*, **385**, 171 (2016); https://doi.org/10.1016/j.apsusc.2016.05.092
21. M. Guillot, C.N. Chinnasamy, J.M. Greneche and V.G. Harris, *J. Appl. Phys.*, **111**, 07A5171 (2012); https://doi.org/10.1063/1.3679020
22. A. Salehabadi, M. Salavati-Niasari, T. Gholami and A. Khoobi, *Int. J. Hydrogen Energy*, **43**, 9713 (2018); https://doi.org/10.1016/j.ijhydene.2018.04.018
23. V. Anbarasu, M. Dhilip, K. Saravana Kumar and K. Sivakumar, *J. Mater. Sci. Mater. Electron.*, **28**, 8976 (2017); https://doi.org/10.1007/s10854-017-6628-9
24. M. Ristic, S. Popovic, I. Czako-Nagy and S. Music, *Mater. Lett.*, **27**, 337 (1996); https://doi.org/10.1016/0167-577X(96)00020-1
25. N. Adhlakha, K.L. Yadav and R. Singh, *Sci. Adv. Mater.*, **5**, 947 (2013); https://doi.org/10.1166/sam.2013.1543
26. G. Madhu, K. Maniammal and V. Biju, *Phys. Chem. Chem. Phys.*, **18**, 12135 (2016); https://doi.org/10.1039/C5CP03710G
27. S. Ghosh, K. Das, K. Chakrabarti and S.K. De, *Dalton Trans.*, **42**, 3434 (2013); https://doi.org/10.1039/C2DT31764H
28. B. Panigrahy, M. Aslam, D.S. Misra, M. Ghosh and D. Bahadur, *Adv. Funct. Mater.*, **20**, 1161 (2010); https://doi.org/10.1002/adfm.200902018
29. V. Anbarasu, A. Manigandan, T. Karthik and K. Sivakumar, *J. Mater. Sci. Mater. Electron.*, **23**, 1201 (2012); https://doi.org/10.1007/s10854-011-0573-9
30. Y. Hamasaki, S. Yasui, T. Katayama, T. Kiguchi, S. Sawai and M. Itoh, *Appl. Phys. Lett.*, **119**, 182904 (2021); https://doi.org/10.1063/5.0063021